Shock wave convergence in water with parabolic wall boundaries

D. Yanuka, D. Shafer, and Ya. Krasik
Physics Department, Technion, Haifa 32000, Israel

(Received 1 March 2015; accepted 21 April 2015; published online 30 April 2015)

The convergence of shock waves in water, where the cross section of the boundaries between which the shock wave propagates is either straight or parabolic, was studied. The shock wave was generated by underwater electrical explosions of planar Cu wire arrays using a high-current generator with a peak output current of ~45 kA and rise time of ~80 ns. The boundaries of the walls between which the shock wave propagates were symmetric along the z axis, which is defined by the direction of the exploding wires. It was shown that with walls having a parabolic cross section, the shock waves converge faster and the pressure in the vicinity of the line of convergence, calculated by two-dimensional hydrodynamic simulations coupled with the equations of state of water and copper, is also larger. © *2015 AIP Publishing LLC*. [http://dx.doi.org/10.1063/1.4919604]

I. INTRODUCTION

Obtaining extreme states of matter is a key issue in research in such fields as inertial confinement fusion,[1] astrophysics,[2] and x-ray lasers.[3] Currently, several approaches are applied to obtain extreme states of matter, for instance, z-pinch,[4] high power lasers,[5] and heavy ion beams.[6] These approaches require expensive experimental setups with stored energy of $\geq 10^5$ J. Recent experiments[7–9] with setups having moderate stored energy of $\leq 6 \times 10^3$ J showed that extreme states of matter can be obtained using either underwater electrical explosion of single wires or converging shock waves (SW) generated by underwater electrical explosion of cylindrical or spherical wire arrays. In the case of the explosion of single wires in water, an energy density up to 500 eV/atom, pressure of $\sim 10^{10}$ Pa, and temperature of a few eV were achieved inside the wires.[10] In the case of converging SW, the largest values of the pressure ($\leq 6 \times 10^{12}$ Pa), density (≤ 9 g/cm^3), and temperature (≤ 16 eV) of the water in the vicinity of the implosion were obtained for a spherical wire array explosion.[9] In these experiments, assuming spherical uniformity of the converging SW and self-similarity of the SW propagation in water, the value of pressure P_{SW} versus the distance from the origin, i.e., radius R_{SW}, increases as $P_{SW} \propto R_{SW}^{-1.33}$, due to fast decrease in the SW surface as $S \propto R_{SW}^2$.

Mdivnishvili *et al.*[11] suggested that using boundaries with a geometry providing faster decrease in the SW surface $S \propto R_{SW}^3$, the parameters (pressure, density, and temperature) of matter in the vicinity of the SW's convergence can be increased as compared with the case of a spherical SW implosion. Indeed, in the case of an adiabatic SW convergence, as the surface of the SW decreases faster, due to energy conservation, the energy density behind the SW front must also increase faster. This leads to a higher pressure gradient and, respectively, to faster propagation velocity. Self-similar analysis and calculations based on the Checter-Chisnell-Witham[12] theory showed similar results, namely, a 1.5 times larger power-law index in super-spherical convergence than in a spherical one. In addition, experimental studies with planar and spherical bounding walls touching each other at the symmetry point showed that indeed the SW generated by the electrical explosion of a ring-surface discharge converges faster than one generated by a cylindrical implosion. These experiments were carried out in air at ~20 μs timescale of the surface discharge duration, which could lead to significant expansion of the discharge channel. The latter can be avoided in underwater electrical explosion of wires because of the near incompressibility of water.

In this paper, we present the results of experiments and two-dimensional (2D) hydrodynamic numerical simulations of the propagation of an SW in water limited by walls having either a straight or parabolic cross section (hereafter called straight/parabolic walls). The SW was generated by the underwater electrical explosion of a planar wire array. The data obtained showed that the SW propagation between parabolic walls was faster and resulted in larger values of pressure at the axis of convergence. Thus, this proof-of-principle experiment showed that indeed parabolic walls contribute to SW propagation velocity, thus suggesting a more complicated experiment where parabolic walls will be used to obtained the SW convergence proportional to R_{SW}^3.

II. EXPERIMENTAL SETUP

A nanosecond timescale, high-voltage generator[13] based on a Marx generator and a water-insulated coaxial forming line producing at the matched load a pulse with voltage and current amplitudes of ~110 kV and ~70 kA, respectively, and pulse duration of ~80 ns at full width at half maximum was used for the explosion of the planar wire array. The scheme of the experimental setup is shown in Fig. 1(a).

The array, consisting of eight wires, each of 63 μm in diameter and 4 cm in length, was placed in an experimental chamber at a distance of ~5.65 mm above the axis of two stainless steel walls of either straight or parabolic form, which were grounded and connected to each other (see Fig. 1(b)). The height (the distance between the axis and the top of the walls) and width of both straight and parabolic walls were 5 mm and 30 mm, respectively. This array was connected between the cathode holder and the grounded electrode via a current viewing resistor (CVR). The experimental chamber,

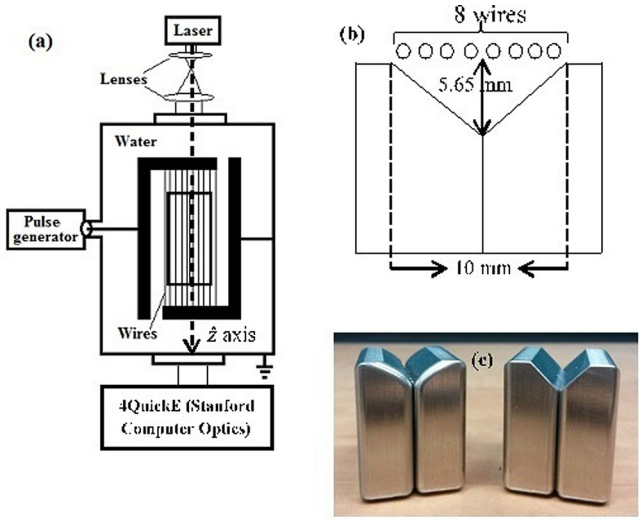

FIG. 1. (a) Experimental setup. (b) Two straight-wedge walls from optical observation viewpoint (along the z axis). (c) Left—parabolic walls. Right—straight walls.

which had two windows for optical observations, was filled with tap water with resistivity of $\sim 4\,\mathrm{k\Omega\cdot cm}$. Tap water was used to prevent high frequency oscillations on the measured voltage waveform, caused by the reflection of an electromagnetic wave while it propagates in the experimental chamber along the cathode holder and wire array having different wave impedances. However, due to relatively low resistivity of water, $\leq 10\%$ of the input current was flowing through it. A capacitive voltage divider and CVR were used to measure the discharge voltage and current, respectively. A continuous wave laser (20 mW, $\lambda = 532\,\mathrm{nm}$) was used for backlighting the generated SW through the windows. Shadowgraph images were captured using a 4QuickE (Stanford Computer Optics, Munich, Germany) fast framing (frame duration of 5 ns) camera (see Fig. 1(a)) at different time delays with respect to the beginning of the SW propagation.

III. EXPERIMENTAL RESULTS

To obtain the operation of the generator with the largest energy density deposition into the exploding wires, the optimal diameter, length and number of wires were first roughly estimated. The diameter D and number n of wires were estimated using the specific current action integral $h = S^{-2}\int_0^{t_{exp}} I^2(t)dt$, where $S = nS_0$ is the total cross-section area of the wires, $S_0 = \pi D_0$ is the cross-sectional area of a single wire, and $I(t)$ is the discharge current. The length of the wires was estimated using energy necessary for the wires to complete evaporation and which should be in the range of $\eta = (20\text{–}30)\%$ of the initial energy W_0 stored in the pulse generator: $l \approx \eta W_0/(\lambda_{ev} n S_0 \rho_{Cu})$, where λ_{ev} is the specific energy density for evaporation and ρ_{Cu} is the specific density of copper. Then, a final selection of the wires was determined by conducting several experiments using varying wire diameters and numbers. These parameters of wires allow one to obtain an almost aperiodic discharge, where $\sim 80\%$ of the stored energy is delivered to the exploding wire array during approximately a quarter of a period of the discharge. Here, let us note that due to the small compressibility of water (adiabatic index $\gamma = 7.15$), the exploding wire expansion is $\sim 10^2$ times slower than in the case of a wire explosion in vacuum or gas. Thus, the decrease in density of the exploding wire during its explosion is not significant, preventing the fast increase of thermal instabilities.[14] Similarly, the $m = 0$ magnetohydrodynamic instability does not have sufficient time to be developed due to the rather large density of the wire and nanosecond timescale of the discharge current. Other magnetohydrodynamic instabilities with $m \geq 1$ require larger timescales to be developed, especially in the case of water as a background medium. In addition, estimates showed that in spite of tens of nanoseconds rise-time of the current, the skin effect is not pronounced due to a small (tens of microns) diameter of the wire and ns-time scale of wire heating leading to fast increase in the resistance of wires.

Typical waveforms of the discharge current and resistive voltage, together with the calculated power and energy deposition into the wires, are shown in Fig. 2. For power and energy calculations, the measured voltage was corrected on inductive voltage $\varphi_{in} = L(dI/dt)$ to calculate resistive voltage $\varphi_r = \varphi - \varphi_{in}$. Here, L is the inductance of the cathode holder and load measured in generator shots with a short-circuit load having inductance similar to that of the wire array. It can be seen that in the generator shot with the wire array explosion, the rise time of the output pulse of the generator was $\sim 80\,\mathrm{ns}$ with a $\sim 45\,\mathrm{kA}$ peak current (current density of $\sim 2 \times 10^8\,\mathrm{A/cm^2}$) and $\sim 80\,\mathrm{kV}$ peak resistive voltage. In addition, it can be seen that the main energy density deposition occurs within $\sim 80\,\mathrm{ns}$ with a deposited energy density of $\sim 7\,\mathrm{kJ/g}$ and peak power of $\sim 2.8\,\mathrm{GW}$. The energy deposition process into the wire consists of several stages, namely, the heating, melting, vaporization, and plasma formation. During the first three stages, the wire array resistance increases up to $\sim 2.5\,\Omega$ right before the explosion, i.e., each wire increases its resistance up to $\sim 20\,\Omega$. Here, by explosion we mean transition of the discharge channel from liquid-vapor to vapor-plasma states of copper, with resistivity determined mainly by electron-neutral collisions and depending on temperature as $T^{-1/2}$.[15] Thus, one can state that the wire explosion is characterized by the formation of a low-ionized and non-ideal (coupling parameter of >1) plasma. The decrease in the discharge current is accompanied by a $\sim 2 \times 10^5\,\mathrm{cm/s}$ radial expansion of the wires. The latter leads to the formation of a compressed and shocked water layer around the wire, and consequently to the formation of an expanding SW. The overlapping of these SWs, generated by all of the wires in the array, leads to the formation of a single planar SW propagating in water with either straight or parabolic boundaries.

Typical shadow images of SWs are shown in Fig. 3 for the two different boundary geometries. Cu wires were welded between the "teeth" electrodes shown in Figs. 3(a) and 3(c). Two overlapping shadow images of the SW front (indicated by white arrows) obtained at different time delays τ_d with respect to the beginning of the discharge current are shown in Figs. 3(b) and 3(d). Here, let us note that at shorter time delays, the SW front is less symmetric than at longer time delays. This effect does not relate to the difference

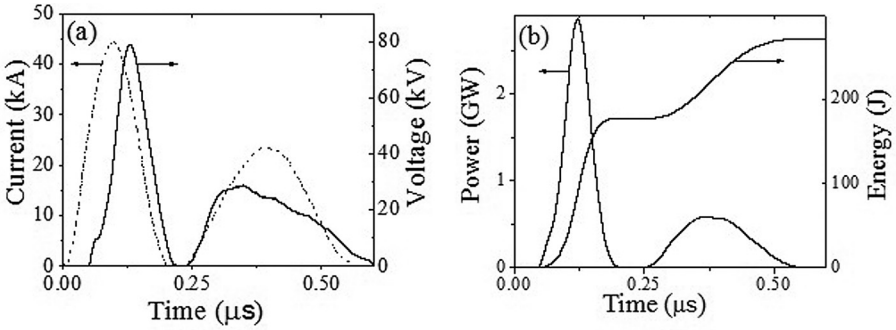

FIG. 2. (a) Current and resistive voltage measured by a CVR and a capacitive voltage divider, respectively. (b) Calculated power and energy.

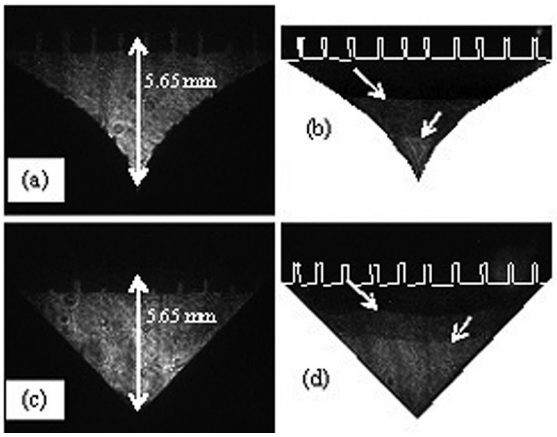

FIG. 3. (a) Image of teeth electrodes and parabolic walls; (b) two overlapping frames of SW propagation with parabolic walls obtained at $\tau_d \sim 700$ ns and $\tau_d \sim 1200$ ns; (c) image of teeth electrodes and straight walls; and (d) two overlapping frames of SW propagation with straight walls obtained at $\tau_d \sim 1700$ ns and $\tau_d \sim 2200$ ns.

between boundary geometries and could be related to some non-uniformity in the stretching of the Cu wires.

The obtained time-of-flight (TOF) data of the SW propagation in water with different boundary geometries are shown in Fig. 4. It can be seen that at $\tau_d \leq 2\,\mu$s, the velocity of SWs propagating in water between parabolic and straight walls is similar and its value is $\sim 1.8 \times 10^5$ cm/s. However, at larger values of τ_d, the velocity of the SW propagating in water between parabolic walls exceeds the velocity of the SW propagating in water between straight walls. The maximum values

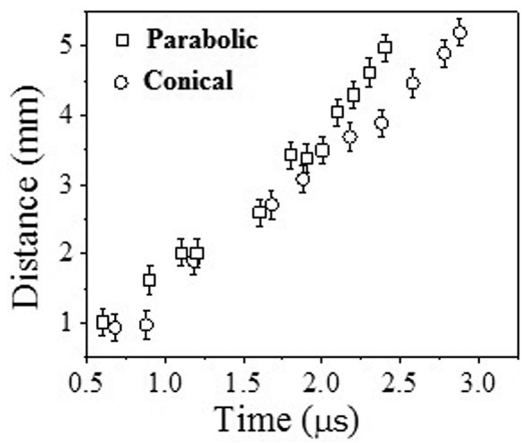

FIG. 4. Distance of the SW front from the exploding wires versus the time from the beginning of the discharge current.

of the SW velocity calculated using the obtained shadow images of the SW front and the known time difference between frames were $\sim 2.9 \times 10^5$ cm/s and 5.4×10^5 cm/s for the SWs propagating in water between straight and parabolic walls, respectively. Thus, the TOF results showed that indeed the application of parabolic boundaries results in faster SW propagation velocity as compared with the case of straight boundaries. Qualitatively, this can be explained by the cross-sectional area of water which SW penetrates in direction of its convergence decreasing differently in case of straight and parabolic boundaries. In the case of rigid boundaries, due to almost complete reflection of the SW, the energy density behind the front of the SW increases. This increase in the energy density, which is larger in the case of parabolic walls, leads to larger density and pressure behind the SW front, and consequently to faster SW propagation velocity.

IV. DISCUSSION

To estimate the parameters of water in the vicinity of the line of convergence, the 2D hydrodynamic numerical simulation described in Ref. 16 was used. The simulation is based on the finite volume method and uses conservation laws of mass, energy, and momentum coupled with the equations of state (EOS) of water and copper.[17] The cross sections of the geometries discussed in Sec. III were divided into a triangular mesh using the Delaunay triangulation algorithm.[18] Each triangle in the mesh contained information of pressure, temperature, density, and specific energy, and the dots where the triangles meet contained information of velocity, position, and acceleration. HD simulations take into account boundary conditions, i.e., when a shock wave propagating in water approaches the boundary. The boundary condition imposed on the frame of the mesh was $v_\perp = 0$, where $v_\perp$ is the transverse velocity of water.

The three conservation law equations are

$$\frac{d}{dt}\int \rho dV = 0, \tag{1}$$

$$\frac{d}{dt}\int \rho \vec{v} dV - \int (P+Q)\vec{n} dA = 0, \tag{2}$$

$$\frac{d\varepsilon}{dt} + (P+Q)\frac{d}{dt}\left(\frac{1}{\rho}\right) = 0, \tag{3}$$

where $\rho, \vec{v}, P, \varepsilon$ are density, velocity, pressure, and specific energy, respectively. Q is the artificial viscosity that was added at each time step to smooth the SW front over several

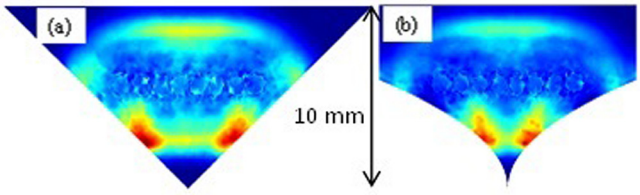

FIG. 5. Snapshots of simulation at $\tau_d = 1.5\,\mu$s: (a) straight walls and (b) parabolic walls. The different colors represent deviations from 10^5 Pa, with the red colors being the largest deviation (~600 MPa). The main increment of pressure is obtained only at the origin.

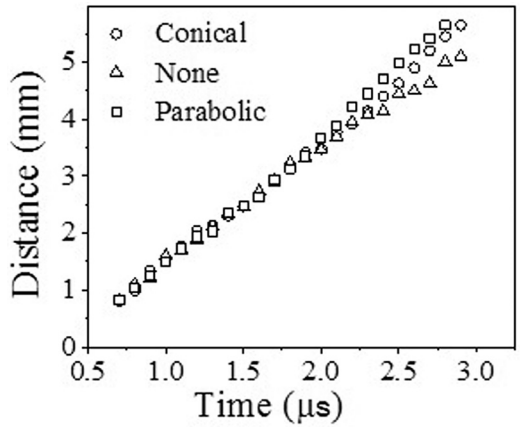

FIG. 6. Simulated TOF of the SW. $t = 0$ is the beginning of the energy deposition into the wires.

mesh triangles for the differential equations' solution to be valid. This viscosity was calculated using the generalized form developed at the Lawrence Livermore Laboratory.[19] In the 2D case, the volume integrals become surface integrals over the triangles and the area integral becomes a line integral over the triangle sides. Equation (1) states that the mass of each triangle does not change during the simulation. Using the known value of pressure at every triangle, the movement of the dots was calculated using Eq. (2), and then, the specific energy was calculated using Eq. (3). The only inputs to the simulation were the experimentally obtained energy deposition into the wires and the EOS of water and copper.

Snapshots of the pressure values from the simulation for both (straight and parabolic) geometries at $\tau_d = 1.5\,\mu$s are presented in Fig. 5. It can be seen that at $\tau_d = 1.5\,\mu$s, the eight Cu wires undergo radial expansion and the SW propagates slightly farther in the case of parabolic walls than that of straight walls. The simulated TOF data of the SWs' propagation for the two geometries are shown in Fig. 6. One can see that at $\tau_d \geq 2\,\mu$s, the velocity of the SW in the case of parabolic walls becomes larger than the velocity of the SW in the case of straight walls, which agrees with the experimental data. Fig. 6 also shows the simulated TOF data of the SWs propagation without any walls, to verify the validity of the simulation, and indeed, the velocity of the propagation of the SW without any walls is found to be significantly smaller, at $\tau_d \geq 2.5\,\mu$s.

The temporal evolution of the pressure for the considered boundary geometries at a distance of 150 μm from the axis of implosion is shown in Fig. 7. It can be seen that the pressure reaches its peak ~180 ns earlier and the value of the pressure is ~5 times higher in the case of parabolic walls. The Rankine-Hugoniot relations[20] for the Mach number of the SW velocity and EOS for water were used to compare the pressure calculated in the simulation to the experimental results

$$M = \sqrt{\delta \frac{(\delta^n - 1)}{n(\delta - 1)}}, \tag{4}$$

$$P - P_0 = 3 \times 10^8 (\delta^n - 1)\,[\text{Pa}]\,, \tag{5}$$

where $\delta \equiv \rho/\rho_0$ is the water compression, ρ and ρ_0 are the density of water behind the SW front and at normal conditions, respectively, $n = 7.15$ is the adiabatic index for water, and M is the Mach number of the water flow. The values of pressure calculated using Eqs. (4) and (5) and the value of M obtained from the experimentally measured TOF of the SW for both straight and parabolic boundaries are $P^{\text{Exp}}_{\text{straight}}(R_{SW} = 0.6 \pm 0.2\,\text{mm}) = 2.2 \pm 0.6\,\text{GPa}$ and $P^{\text{Exp}}_{\text{Parabolic}}(R_{SW} = 1.05 \pm 0.2\,\text{mm}) = 3.57 \pm 0.6\,\text{GPa}$. The values of pressure obtained by 2D simulations are $P^{\text{Sim}}_{\text{straight}}(R_{SW} = 0.6\,\text{mm}) = 2.26\,\text{GPa}$ and $P^{\text{Sim}}_{\text{Parabolic}}(R_{SW} = 1.05\,\text{mm}) = 4.19\,\text{GPa}$. One can see a rather good agreement between experimental and numerical results showing that in the parabolic case, the pressure behind the front of the SW is larger in the case of the SW convergence in water with parabolic boundaries.

V. SUMMARY

To summarize, carried out experimental and 2D hydrodynamic numerical investigation showed that the application

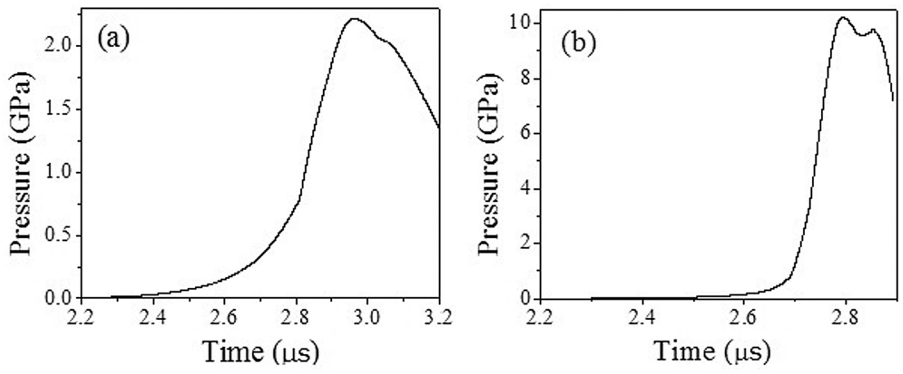

FIG. 7. Temporal evolution of the pressure at a distance of 150 μm. (a) Straight walls and (b) parabolic walls.

of parabolic walls contributes to an increase in the water parameters at the line of convergence of an SW generated by the underwater electrical explosion of a planar wire array. We are planning to study SW implosion in azimuthally symmetrical parabolic geometry, and we expect to obtain greater values of pressure at the vicinity of convergence than in the case of a spherical converging SW.

ACKNOWLEDGMENTS

Authors are grateful to Dr. Sergey Efimov, Dr. Victor Gurovich, and Oleg Antonov for discussions and fruitful comments and Svetlana Gleizer and Kalman Gruzinski for technical assistance. This research was supported by the Israeli Science Foundation Grant No. 99/12.

[1]T. Ma, P. K. Patel, N. Izumi, P. T. Springer, M. H. Key, L. J. Atherton, L. R. Benedetti, D. K. Bradley, D. A. Callahan, P. M. Celliers, C. J. Cerjan, D. S. Clark, E. L. Dewald, S. N. Dixit, T. Doppner, D. H. Edgell, R. Epstein, S. Glenn, G. Grim, S. W. Haan, B. A. Hammel, D. Hicks, W. W. Hsing, O. S. Jones, S. F. Khan, J. D. Kilkenny, J. L. Kline, G. A. Kyrala, O. L. Landen, S. Le Pape, B. J. MacGowan, A. J. Mackinnon, A. G. MacPhee, N. B. Meezan, J. D. Moody, A. Pak, T. Parham, H.-S. Park, J. E. Ralph, S. P. Regan, B. A. Remington, H. F. Robey, J. S. Ross, B. K. Spears, V. Smalyuk, L. J. Suter, R. Tommasini, R. P. Town, S. V. Weber, J. D. Lindl, M. J. Edwards, S. H. Glenzer, and E. I. Moses, Phys. Rev. Lett. **111**, 085004 (2013).
[2]K. K. Reeves and L. Golub, Astrophys. J., Lett. **727**, L52 (2011).
[3]J. J. Rocca, V. Shlyaptsev, F. G. Tomasel, O. D. Cortazar, D. Hartshorn, and J. L. A. Chilla, Phys. Rev. Lett. **73**, 2192 (1994).
[4]I. M. Hall, T. Durmaz, R. C. Mancini, J. E. Bailey, G. A. Rochau, I. E. Golovkin, and J. J. MacFarlane, Phys. Plasmas **21**, 031203 (2014).
[5]B. A. Remington, R. P. Drake, and D. D. Ryutov, Rev. Mod. Phys. **78**, 755 (2006).
[6]N. A. Tahir, D. H. H. Hoffmann, A. Kozyreva, A. Shutov, J. A. Maruhn, U. Neuner, A. Tauschwitz, P. Spiller, and R. Bock, Phys. Rev. E **61**, 1975 (2000).
[7]D. Sheftman, D. Shafer, S. Efimov, K. Gruzinsky, S. Gleizer, and Ya. E. Krasik, Rev. Sci. Instrum. **83**, 103505 (2012).
[8]A. Fedotov-Gefen, S. Efimov, L. Gilburd, G. Bazalitski, V. Tz. Gurovich, and Ya. E. Krasik, Phys. Plasmas **18**, 062701 (2011).
[9]O. Antonov, S. Efimov, D. Yanuka, M. Kozlov, V. Tz. Gurovich, and Ya. E. Krasik, Appl. Phys. Lett. **102**, 124104 (2013).
[10]A. Grinenko, S. Efimov, A. Fedotov, and Ya. E. Krasik, Phys. Plasmas **13**, 052703 (2006).
[11]M. O. Mdivnishvili, I. V. Sokolov, M. I. Taktakishvili, and P. A. Voinovich, Shock Waves **9**, 149–158 (1999).
[12]G. B. Whitham, *Linear and Nonlinear Waves* (Wiley, New York, 1974).
[13]A. Grinenko, Ya. E. Krasik, S. Efimov, V. Tz. Gurovich, and V. I. Oreshkin, Phys. Plasmas **13**, 042701 (2006).
[14]A. G. Rousskikh, V. I. Oreshkin, S. A. Chaikovsky, N. A. Labetskaya, A. V. Shishlov, I. I. Beilis, and R. B. Baksht, Phys. Plasmas **15**, 102706 (2008).
[15]Y. P. Raizer, *Gas Discharge Physics* (Springer-Verlag, Berlin, Heidelberg, 1991).
[16]M. Kozlov, V. Tz. Gurovich, and Ya. E. Krasik, Phys. Plasmas **20**, 112701 (2013).
[17]See National Technical Information Service Document No. DE85014241 (S. P. Lyon and J. D. Johnson, Sesame: The Los Alamos National Laboratory Equation-of-State Database, LANL Report No. LA-UR-92-3407, 1992). Copies may be ordered from the National Technical Information Service, Springfield, VA, 22161.
[18]D. T. Lee and B. J. Schachter, Int. J. Comput. Inf. Sci. **9**(3), 219 (1980).
[19]Tz. V. Kolev and R. N. Rieben, J. Comput. Phys. **228**, 8336–8366 (2009).
[20]Ya. B. Zel'dovich and Yu. P. Raizer, *Physics of Shock Waves and High-Temperature Hydrodynamic Phenomena* (Academic Press, New York, London, 1966).